PMSM Vector Control Strategy Based on Active Disturbance Rejection Controller

Kai Zhou [1], Min Ai [1,*], Yancheng Sun [2], Xiaogang Wu [1] and **Ran Li [1]**

[1] Engineering Research Center of Automotive Electronics Drive Control and System Integration, Ministry of Education, Harbin University of Science and Technology, Harbin 150080, China; zhoukai@hrbust.edu.cn (K.Z.); xgwu@hrbust.edu.cn (X.W.); zeemoolr@126.com (R.L.)
[2] State Grid Beijing Electric Power Company, Beijing 100000, China; sycjack@sina.com
* Correspondence: aimin_tx@163.com; Tel.: +86-18-845-116-848

Abstract: Based on current research into the vector control principles of the permanent magnet synchronous motor (PMSM), a control strategy founded upon an Active Disturbances Rejection Controller (ADRC) is proposed. This control strategy consists of an ADRC speed loop and current controller. By studying the factors affecting the running state of a PMSM, a mathematical model is established, and the design principle of the active disturbances rejection controller is analyzed in order to design the ADRC speed loop. The speed loop considers errors caused by uncertain factors, such as external disturbances, to be the disturbance amount, which is observed and then compensated for by the ADRC, thereby improving the dynamic and static performance as well as the anti-disturbance capability of the system. In order to achieve the strong coupling of the PMSM, the current controller was also designed to decouple the d–q axis current. Our simulation and experimental results demonstrate the feasibility and practicability of this control strategy.

Keywords: permanent magnet synchronous motor; vector control; active disturbance rejection controller; feedback linearization

1. Introduction

The energy crisis and environmental issues which characterize the early 21st Century have been generating fear and uncertainty worldwide [1]. As awareness grows that our continued reliance upon fossil fuels is untenable, the traditional automotive industry has suffered, and electric vehicles powered by alternative energy have emerged as an increasingly popular alternative [2]. The permanent magnet synchronous motor (PMSM) has been widely promoted within the field of electric vehicles, as it possesses a number of desirable characteristics, including a small torque ripple, a wide speed range, a simple structure, a large torque inertia and low vibration noise [3–5]. As the in-depth study of PMSM control systems has progressed, a variety of advanced control strategies have been proposed, including a synovial deformation structure, time optimal control, adaptive control and nonlinear proportional–integral–derivative (PID) [6,7]. However, the control effect of most strategies depends upon the precise model of the controlled object, which is more complicated and difficult to implement. Artificial intelligence control has become a hot topic in current research because of its strong robustness and also remaining independent of the controlled object model. The complexity of the algorithm, and the large amount of computation, limit its application in the actual control system. The PI controller is widely used in the speed loop and current loop of the control system due to its simple structure and easy implementation. But the control performance in the time-varying system is weak, and there are problems such as overshoot, which make it difficult to achieve high-precision control [8,9].

The Active Disturbances Rejection Controller (ADRC) was developed by the researcher Han Jingqing of the Chinese Academy of Sciences following in-depth research into modern control theory [10–14]. It combines PID control technology based on error feedback, using this to eliminate the essence of error control, and thereby proposing a new, nonlinear, practical control method [10–12,15]. The ADRC suppresses overshoot by means of the Tracking Differentiator (TD) design transition process during operation, and observes the external disturbance and parameter variation of the system through the Extended State Observer (ESO) [13,14,16]. The ESO accounts for the defects of the PID controller and results in the accelerated convergence of any error, as well as possessing desirable dynamic and static characteristics [17].

This paper investigates the PMSM, and from the analysis of its topology and principles, a control strategy based on an ADRC is proposed. Since the PMSM is a complex nonlinear system, favorable control performance can be obtained by decoupling the coupling term in its mathematical equation. The commonly-used PI control decoupling is difficult to meet the performance requirements in the full speed range. Therefore, the feedback linearization theory is applied. The Lie differential operation of the output variable is used to obtain the required coordinate transformation and nonlinear system state feedback. The input-output feedback linearization of the PMSM is realized, and the feedback linearization algorithm is designed. The controller implements the decoupling control of the system. Our simulation and experimental research into the control system demonstrate that our proposed control strategy is robust, and exhibits both stable and accurate dynamic tracking.

This paper is organized as follows: The design of ADRC is given in Section 2. In Section 3, the current decoupling controller and the magnetic chain observer are given. Section 4 provides simulation and experimental results. Section 5 concludes this paper.

2. The Active Disturbances Rejection Controller

Active disturbances rejection controller technology is a nonlinear control strategy. It combines classical adjustment theory with modern control theory, and has the advantages of simple algorithm and easy adjustment [18]. This control theory applies nonlinear feedback to the control system to compensate for errors caused by uncertainties such as internal and external disturbances. Moreover, the active disturbances rejection controller technology has a low dependence on the accuracy of the mathematical model of the controlled system, so it has unique advantages in dealing with the nonlinear control system. The active disturbances rejection controller mainly includes three parts: The tracking differentiator (TD), extended state observer (ESO) and nonlinear state error feedback (NLSEF) [19].

Since the auto-disturbance technique can be applied to an uncertain object that is affected by an unknown disturbance, it is described by the following differential equation.

$$\begin{cases} x^{(n)} = f(x, \dot{x}, \cdots, x^{(n-1)}, t) + d(t) + bu(t) \\ y = x(t) \end{cases} \tag{1}$$

Where: $f(x, \dot{x}, \cdots, x^{(n-1)}, t)$ is an unknown function; $d(t)$ is an unknown disturbance; y is the system output; $u(t)$ is the system control quantity; b is the gain of control input.

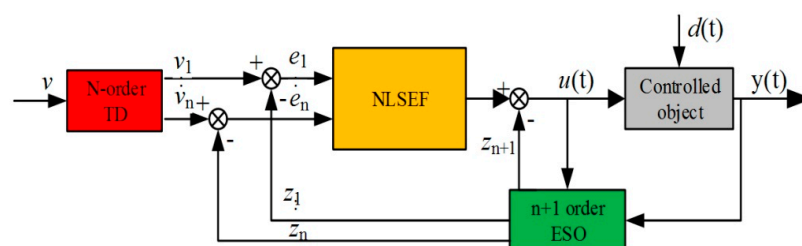The schematic diagram of the standard active disturbances rejection controller is shown in Figure 1.

Figure 1. Active disturbance rejection control system structure principle diagram.

2.1. Tracking Differentiator

The tracking differentiator is the first part of the auto-disturbance controller. The tracking transition process effectively solves the problem that the super-adjustment and rapidity of the classical PID control technology have difficulty in coordinating in the control system, and reduces the overshoot of the system. It enables it to track the system reference input quickly, while obtaining an approximate differential signal according to the order of the controller [20–23]. The second order differential equation is:

$$\begin{cases} \dot{z}_1 = z_2 \\ \dot{z}_2 = f(z_1, z_2) \end{cases} \tag{2}$$

All solutions are bounded and satisfied by:

$$\begin{cases} \lim_{t\to\infty} z_1(t) = 0 \\ \lim_{t\to\infty} z_2(t) = 0 \end{cases} \tag{3}$$

For any bounded measurable signal $v(t)$, $t \in [0, \infty]$ and arbitrary $T > 0$, differential equation is:

$$\begin{cases} \dot{x} = x_2 \\ \dot{x} = r^2 f(x - v(t), \frac{x_2}{r}) \end{cases} \tag{4}$$

The first component of the solution $x_1(r, t)$ is satisfied by:

$$\lim \int_0^T |x1(r,t) - v(t)| dt = 0 \tag{5}$$

Extend the above equation to the nth order system, the dynamic system is set up:

$$\begin{cases} \dot{z}_1 = z_2 \\ \vdots \\ \dot{z}_{n-1} = z_n \\ \dot{z}_n = f(z_1, z_2, \cdots, z_n) \end{cases} \tag{6}$$

Where any solution is asymptotically stable at the origin, and all solutions are satisfied by $\lim z_i(t) = 0, i = 1, 2, \cdots, n$. Then, for any locally integrable signal $v(t)$, with $t \in [0, \infty)$, and any $T > 0$, the new dynamic system for any bounded integrable function $v(t)$ is:

$$\begin{cases} \dot{x}_1 = x_2 \\ \vdots \\ \dot{x}_{n-1} = x_n \\ \dot{x}_n = r^n f(x_1 - v(t), \frac{x_2}{r}, \cdots \frac{x_n}{r^{n-1}}) \end{cases} \tag{7}$$

Solution satisfies: $\lim_{r\to\infty} \int_0^T |x_1(t) - v(t)| dt = 0$. As r increases, the system solution can fully approximate a given input signal for a limited time.

2.2. Extended State Observer

The system always exchanges information with the environment during its operation. For a dynamic system, the external variable of the system is the output variable of the system to the outside. The device that determines the state variable inside the system according to the observation of the external variable is the state observer, and it determines the system according to the measured system input and system output. The extended state observer is, in a sense, a versatile and applicable disturbance observer.

Set the second-order linear control system as:

$$\begin{cases} \dot{x}_1 = x_2 \\ \dot{x}_2 = a_1 x_1 + a_2 x_2 + bu \\ y = x_1 \end{cases} \tag{8}$$

The corresponding system state observer is:

$$\begin{cases} e_1 = z_1 - y \\ \dot{z}_1 = z_2 - l_1 e_1 \\ \dot{z}_2 = (a_1 z_1 + a_2 z_2) - l_2 e_1 + bu \end{cases} \tag{9}$$

The error equation between the system and the original system is:

$$\begin{cases} e_1 = z_1 - x_1, e_2 = z_2 - x_2 \\ \dot{e}_1 = -l_1 e_1 + e_2 \\ \dot{e}_2 = (-l_2 + a_1)e_1 + a_2 e_2 + bu \end{cases} \tag{10}$$

Select l_1, l_2 to make matrix $\begin{bmatrix} -l_1 & 1 \\ -l_2 & a_2 \end{bmatrix}$ stable; the Equation (9) is the state observer of the Equation (8).

Nonlinear system is:

$$\begin{cases} \dot{x}_1 = x_2 \\ \dot{x}_2 = f(x_1, x_2) + bu \\ y = x_1 \end{cases} \tag{11}$$

When $f(x_1, x_2)$ and b are determined, the following state observer is established:

$$\begin{cases} e_1 = z_1 - y \\ \dot{z}_1 = z_2 - l_1 e_1 \\ \dot{z}_2 = f(z_1, z_2) - l_2 e_1 + bu \end{cases} \tag{12}$$

The error equation for the Equation (12) is:

$$\begin{cases} e_1 = z_1 - x_1, e_2 = z_2 - x_2 \\ \dot{e}_1 = e_2 - l_1 e_1 \\ \dot{e}_2 = f(x_1 + e_1, x_2 + e_2) - f(x_1, x_2) - l_2 e_1 \end{cases} \tag{13}$$

Assuming that $f(x_1, x_2)$ is continuously differentiable, it is linearly approximated by a Taylor expansion:

$$\begin{cases} e_1 = z_1 - x_1, e_2 = z_2 - x_2 \\ \dot{e}_1 = e_2 - l_1 e_1 \\ \dot{e}_2 = \frac{\partial f(x_1, x_2)}{\partial x_1} e1 + \frac{\partial f(x_1, x_2)}{\partial x_2} e_2 - l_2 e_1 \end{cases} \tag{14}$$

As long as $\frac{\partial f(x_1, x_2)}{\partial x_1}$ and $\frac{\partial f(x_1, x_2)}{\partial x_2}$ are bounded, l_1 and l_2 can always be determined, and if the error Equation (14) is stable, Equation (12) will become the state observer of the Equation (11).

Define $x_3(t) = f(x_1(t), x_2(t))$ and $\dot{x}_3(t) = w(t)$, then Equation (11) can be expanded into a new linear control system:

$$\begin{cases} \dot{x}_1 = x_2 \\ \dot{x}_2 = x_3 + bu \\ \dot{x}_3 = w(t) \\ y = x_1 \end{cases} \tag{15}$$

Establish a state observer for the expanded system:

$$\begin{cases} e_1 = z_1 - y \\ \dot{z}_1 = z_2 - \beta_1 e_1 \\ \dot{z}_2 = z_3 - \beta_2 |e_1|^{\frac{1}{2}} sign(e_1) + bu \\ \dot{z}_3 = -\beta_3 |e_1|^{\frac{1}{4}} sign(e_1) \end{cases} \tag{16}$$

By selecting the appropriate parameters β_1, β_2 and β_3, the system can estimate the state variables $x_1(t)$ and $x_2(t)$ and the real-time effect $x_3(t)$ of the expanded state. The state observer of the expanded Equation (16) is called the state observer, and $x_3(t)$ is called the expanded state.

The extended state observer obtains the tracking signal $z_1(t)$ of the system output signal $y(t)$ and the derivative signal $z_i(t)$ of each order, and the system disturbance estimation signal $z_{n+1}(t)$ to estimate the disturbance. Extend the external disturbance and model error to a new state variable. According to the classical state observer principle, the following equation can be obtained:

$$\begin{cases} e = z_1 - y \\ \dot{z}_1 = z_2 + g_1(e) \\ \vdots \\ \dot{z}_{n-1} = f(x_1, \cdots, x_{n-1}) + bu + g_{n-1}(e) \\ \dot{z}_n = g_n(e) \end{cases} \tag{17}$$

Select the appropriate function to observe the state variables and total disturbances of the system.

2.3. Nonlinear State Error Feedback Controller

The nonlinear structure and control parameters play a key role in the fast convergence of the auto disturbance rejection controller to the target. "Feedback" is the essence of control theory. The feedback mechanism can improve the performance of the system. It can change a linearly-controlled system into a nonlinear-controlled system, and vice versa. The feedback mechanism in the negative feedback-controlled system also has the ability to restrain small, uncertain disturbances. The most breakthrough idea of self-disturbance control is to explore the potential of the feedback mechanism as much as possible, and to exert its control and anti-interference ability.

The tracking differentiator and the extended state observer respectively generate tracking signals and state variables. The nonlinear state error feedback controller uses a function to solve the control quantity structure by using the functions of the above two parameters.

The general form is as follows:

$$\begin{cases} e_1 = v_1 - z_1 \\ \vdots \\ e_n = v_n - z_n \\ u_0(t) = k_1 f_1(e_1, t) + \cdots + k_n f_n(e_n, t) \\ u(t) = u_0(t) - z_{n+1}(t)/b \end{cases} \tag{18}$$

Where: $e_i(i = 1,2,...,n)$ is the difference between the tracking signal and the state variable estimate; $f_i(e_i, t)$ is a nonlinear function; $u_0(t)$ is the system control quantity; $-z_{n+1}(t)/b$ acts to compensate for the disturbance.

3. Design of ADRC

The classic permanent magnet synchronous motor $i_d{}^* = 0$ vector control strategy usually adopts the double loop control structure, where the inner loop is the current loop, and the outer loop is the

speed loop. At this time, the principle structure diagram of the vector control speed control system of the permanent magnet synchronous motor based on $i_d{}^* = 0$ is shown in Figure 2 [23–26].
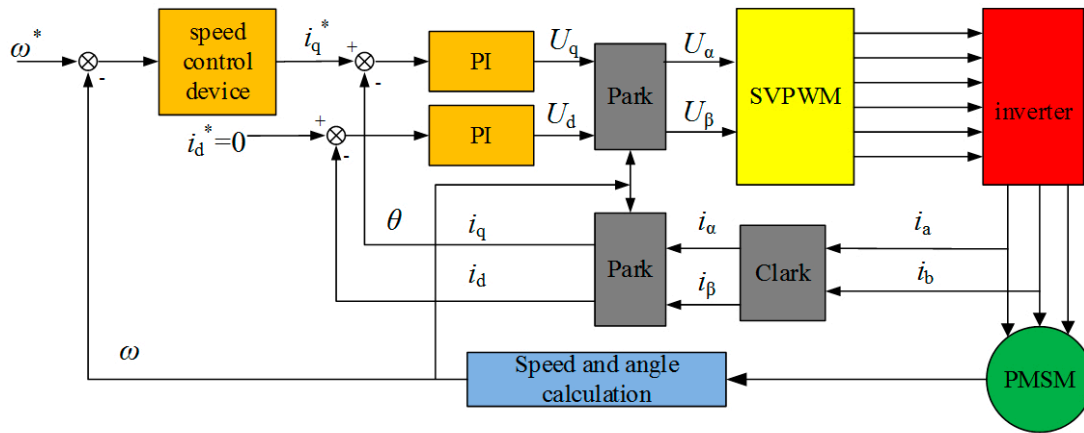

Figure 2. Double closed loop vector control of the permanent magnet synchronous motor (PMSM) principle diagram.

In order to facilitate the analysis and application, the interference of the core parameters, such as core saturation, higher harmonics and eddy current on the motor parameters, is temporarily ignored. The voltage equation of the PMSM in the synchronous rotating coordinate system is as follows:

$$u_d = R_s i_d + \frac{d}{dt}\psi_d - \omega_e \psi_q \tag{19}$$

$$u_q = R_s i_q + \frac{d}{dt}\psi_q + \omega_e \psi_d \tag{20}$$

The flux linkage equation is:

$$\psi_d = L_d i_d + \psi_f \tag{21}$$

$$\psi_q = L_q i_q \tag{22}$$

Based upon the theory of magnetic field orientation, the state equation of a PMSM in a synchronous rotating coordinate system is [27]:

$$
\begin{bmatrix} \dot{i_d} \\ \dot{i_q} \\ \dot{\omega_e} \end{bmatrix} =
\begin{bmatrix} -R_s/L & n_p\omega_e & 0 \\ n_p\omega_e & -R_s/L & -n_p\psi_f/L \\ 0 & 1.5n_p\psi_f/J & -B/J \end{bmatrix}
\begin{bmatrix} i_d \\ i_q \\ \omega_e \end{bmatrix} +
\begin{bmatrix} u_d/L_d \\ u_q/L_q \\ -T_L/J \end{bmatrix} \tag{23}
$$

Where u_d, u_q, ψ_d, and ψ_q are the stator voltage and flux linkage components in the d–q coordinate system, respectively, and also where i_d and i_q are the direct axis and the intersecting axis current, respectively; L_d is the direct axis and L_q the intersecting axis inductance. Meanwhile, R_s is the stator resistance; ψ_f is the rotor flux; T_L is the load torque; P_n is the motor pole pair; J is the moment of inertia; and ω_e is the rotor angular velocity.

From the design of the auto-disturbance controller on the speed loop, the system state is only the speed. Therefore, only one-order ADRC is needed for this factor, so that the extended state observer is the second-order. In order to facilitate control and reduce the number of controlled parameters, a linear function is used instead of a nonlinear function.

From Equation (23), we can get:

$$\dot{\omega_e} = \frac{3n_p\psi_f i_q}{2J} - \frac{B\omega_e}{J} - \frac{T_L}{J} \tag{24}$$

Set the disturbance:

$$a(t) = -\frac{B}{J}\omega_e - \frac{T_L}{J} \tag{25}$$

$$b = 1.5\frac{n_p\psi_f}{J} \tag{26}$$

Inferred:

$$\dot{\omega} = a(t) + bi_q \tag{27}$$

It can be seen from the above equation that the motion damping coefficient, moment of inertia and external disturbance of the PMSM can be represented in *a(t)*. Consequently, the transition should be arranged in a manner that achieves the real-time tracking of the input signal. At the same time, in order to improve the anti-disturbance ability of the system, *a(t)* should be observed and compensated for. Therefore, the specific structure of the first-order ADRC controller, designed according to the principle of active disturbance rejection, is shown in Figure 3.
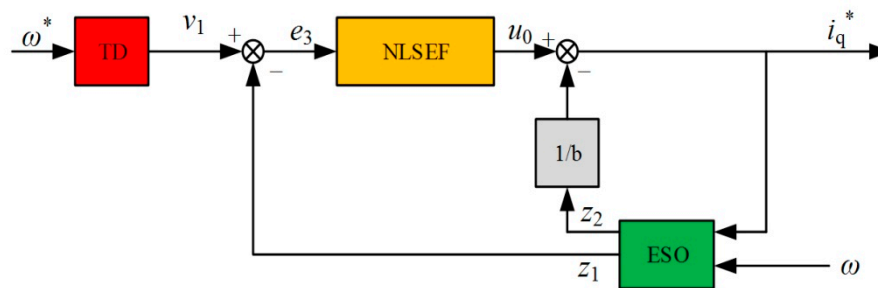

Figure 3. The first order Active Disturbances Rejection Controller (ADRC) structure diagram.

First-order tracking differentiator:
TD:

$$\begin{cases} e_1 = v_1 - \omega^* \\ \dot{v}_1 = -re_1 \end{cases} \tag{28}$$

ESO:

$$\begin{cases} e_1 = z_1 - \omega \\ \dot{z}_1 = z_2 - \beta_1 e_2 + bu \\ \dot{z}_2 = -\beta_2 e_2 \end{cases} \tag{29}$$

NLSEF:

$$\begin{cases} e_3 = v_1 - z_1 \\ u_0 = ke_3 \\ u = u_0 - \frac{z_2}{b} \end{cases} \tag{30}$$

Where: ω^* is the given speed variable; v_1 is the tracking signal; ω is the actual motor speed; z_1 is the observed signal; z_2 is the disturbance feedback.

It can be seen from the above equations that there are r, β_1, β_2 and k in the ADRC control system which are need to be set. It can be seen from Equation (28) that increasing the parameter r in the tracking differentiator can bring the tracking signal closer to a given speed. However, overshoot will occur as r increases, so multiple tunings are required. β_1, and β_2 determine the performance of ESO, which is mainly reflected in the convergence speed. β_2 affects the estimation of disturbances in the ESO system. As the value increases, the system's load-resistance is enhanced. Therefore, the time for the system to return to steady state after the sudden change of the load is short. However, the system oscillation is more obvious when β_2 is over-exposed, so β_1 is increased to restrain the oscillation at this time.

According to the method proposed by Gao Zhiqiang, the system bandwidth and the extended state observer bandwidth are used to reduce the number of tuning parameters. Using the linear

system synthesis method to perform pole assignment on Equation (29), we can derive the characteristic equation as:

$$p(s) = s^2 + \beta_1 s + \beta_2 \tag{31}$$

The necessary and sufficient condition for β_1 and β_2 is that all of the roots of Equation (18) must be on the left plane. If a closed-loop pole is desired $-p(p > 0)$, then:

$$p(s) = (s + p)^2 = s^2 + 2ps + p^2 \tag{32}$$

By using system bandwidth ω_c and extended state observer bandwidth ω_0, the observation poles can be placed on top ω_0:

$$\beta_1 = 2\omega_0, \ \beta_2 = {\omega_0}^2 \tag{33}$$

$$\omega_0 \approx 3 \sim 5\omega_c \tag{34}$$

Only one parameter needs to be set. The larger the tracking signal, the faster the system response. In the experiment, the trial-and-error method was used to adjust the system parameters. In short, the tuning of the four parameters should be coordinated and adjusted. Through the experience and comparative analysis of each simulation, multiple attempts are made to determine the most appropriate parameters.

The pole placement method is currently a widely-used parameter tuning method. It is simple and easy to use, and the parameters are satisfied within a certain range.

4. Current Controller Design

The current controller mainly comprises a current decoupling controller and a flux linkage observer. The decoupling controller applies the feedback linearization theory to decouple the complex coupling terms in the mathematical equations of the motor. The flux observer provides the necessary information for the decoupling controller.

4.1. Current Decoupling Controller

Because the electromagnetic torque of the three-phase permanent magnet synchronous motor is:

$$T_e = 1.5p_n(\psi_d i_q - \psi_q i_d) \tag{35}$$

Where: T_e is the electromagnetic torque.

Substituting Equations (21) and (22) into Equation (31) yields:

$$T_e = 1.5p_n[\psi_f i_q + (L_d - L_q)i_d i_q] \tag{36}$$

Since $L_d = L_q = L$, Equation (32) can be simplified as:

$$T_e = 1.5n_p\psi_f i_q \tag{37}$$

It can be seen from Equation (23) that the PMSM is a multi-variable system. There is a strong nonlinear coupling relationship between i_d, i_q and ω_e, which cannot be adjusted separately. Therefore, i_d and i_q need to be used in order to achieve decoupling.

A rewriting of the system state Equation (23) in the d–q coordinate system to the affine nonlinear standard form is as follows:

$$\dot{x} = f(x) + g_1(x)u_d + g_2(x)u_q \tag{38}$$

$$f(x) = \begin{bmatrix} -R_S i_d + L_q i_q \omega_e \\ -R_S i_q - L_d i_d \omega_e - \omega_e \psi_f \\ (T_e - P_n T_L - B\omega_e)/J \end{bmatrix} \tag{39}$$

$$
\begin{bmatrix} g_1(x) & g_2(x) \end{bmatrix} = \begin{bmatrix} 1 & 0 \\ 0 & 1 \\ 0 & 0 \end{bmatrix} \tag{40}
$$

Before the controller can be designed, the conditions under which the feedback linearization method is established in the direct torque control system must be discussed.

$$
\begin{aligned}
\begin{bmatrix} L_{g_1}\psi_d & L_{g_2}\psi_d \\ L_{g_1}\psi_q & L_{g_2}\psi_q \end{bmatrix} &= \begin{bmatrix} g_1\frac{\partial\psi_d}{\partial x} & g_2\frac{\partial\psi_d}{\partial x} \\ g_1\frac{\partial\psi_q}{\partial x} & g_2\frac{\partial\psi_q}{\partial x} \end{bmatrix} \\
&= \begin{bmatrix} 1 & 0 \\ 0 & 1 \end{bmatrix}
\end{aligned} \tag{41}
$$

The decoupling matrix is a nonsingular matrix that satisfies exact linearization conditions.

To decouple the equations, two virtual control quantities K_1 and K_2 are designed and defined as follows:

$$
\begin{cases} k_1 = \dot{y}_1 = L_f\psi_d + L_{g_1}\psi_d u_d + L_{g_2}\psi_d u_q \\ k_2 = \dot{y}_2 = L_f\psi_q + L_{g_1}\psi_q u_d + L_{g_2}\psi_q u_q \end{cases} \tag{42}
$$

Where: $y_1 = \psi_d$ and $y_2 = \psi_q$. They are system output variables, where $L_f\psi_d$ is the *Li* derivative of ψ_d with respect to f, and the meanings of L_{g1} and L_{g2} are similar, and will not be described again.

Bringing Equations (37) and (38) into Equation (34) yields:

$$
\begin{bmatrix} u_d \\ u_q \end{bmatrix} = \begin{bmatrix} L_{g_1}\psi_d & L_{g_2}\psi_d \\ L_{g_1}\psi_q & L_{g_2}\psi_q \end{bmatrix}^{-1} \begin{bmatrix} k_1 - L_f\psi_d \\ k_2 - L_f\psi_q \end{bmatrix} \tag{43}
$$

In order for the changed linear system outputs ψ_d, ψ_q to track the given signals $\psi_d{}^*$ and $\psi_q{}^*$, the controller is designed to:

$$
\begin{cases} k_1 = \frac{d\psi_d{}^*}{dt} - \alpha_1(\psi_d{}^* - \psi_d) \\ k_2 = \frac{d\psi_q{}^*}{dt} - \alpha_2(\psi_q{}^* - \psi_q) \end{cases} \tag{44}
$$

Where: α_1 and α_2 are controller modulation parameters with positive values. Finished, u_d and u_q can be expressed as:

$$
\begin{cases} u_d = -Ri_d + \omega_e L_q i_q - k_1 \\ u_q = -Ri_q - \omega_e L_d i_d + \omega_e \psi_f - k_2 \end{cases}
$$

$$
\begin{cases} u_d = -Ri_d + \omega_e L_q i_q - k_1 \\ u_q = -Ri_q - \omega_e L_d i_d + \omega_e \psi_f - k_2 \end{cases} \tag{45}
$$

And the flux linkage tracking error equation:

$$
\begin{cases} \frac{d(\psi_d{}^* - \psi_d)}{dt} = -\alpha_1(\psi_d{}^* - \psi_d) \\ \frac{d(\psi_q{}^* - \psi_q)}{dt} = -\alpha_2(\psi_q{}^* - \psi_q) \end{cases} \tag{46}
$$

It can be seen from these equations that the system's steady state error can be reduced to be close to zero by making the controller modulation parameter greater than zero.

4.2. Magnetic Chain Observer

In order to facilitate the observation of the stator flux linkage, it is necessary to rewrite Equations (19) and (20) into a form under the α–β coordinate system. The mathematical model of the permanent magnet synchronous motor in the α–β coordinate system is:

$$
\begin{cases} u_\alpha = (R + Dl)i_\alpha - \omega_e \psi_f \sin\theta \\ u_\beta = (R + DL)i_\beta + \omega_e \psi_f \cos\theta \end{cases} \tag{47}
$$

Where D is a differential operator, θ is the rotor flux point angle, and ω_e is the electrical angular velocity.

Construct extended flux linkage terms $\psi_{\alpha 1}$ and $\psi_{\beta 1}$:

$$\begin{cases} u_{\alpha 1} = \psi_f \cos \theta \\ u_{\beta 1} = \psi_f \sin \theta \end{cases} \tag{48}$$

The extended flux linkage term is used to represent the permanent magnet synchronous motor model:

$$\begin{cases} u_\alpha = (R + Dl)i_\alpha + D\psi_{\alpha 1} \\ u_\beta = (R + DL)i_\beta + D\psi_{\beta 1} \end{cases} \tag{49}$$

Order $x = \psi_{\alpha \beta 1} = \begin{bmatrix} \psi_{\alpha 1} & \psi_{\beta 1} \end{bmatrix}^T$, a new equation of state is available:

$$\begin{cases} \dot{x} = Ax + Bu \\ y = Cx \end{cases} \tag{50}$$

$$\begin{cases} A = \omega_e J = \begin{bmatrix} 0 & -\omega_e \\ \omega_e & 0 \end{bmatrix} \\ B = O = \begin{bmatrix} 0 & 0 \\ 0 & 0 \end{bmatrix} \\ C = \omega_e J = \begin{bmatrix} 0 & -\omega_e \\ \omega_e & 0 \end{bmatrix} \end{cases} \tag{51}$$

The relationship between the stator flux linkage and the extended flux linkage is:

$$\begin{cases} \psi_\alpha = Li_\alpha + \psi_{\alpha 1} \\ \psi_\beta = Li_\beta + \psi_{\beta 1} \end{cases} \tag{52}$$

The electromagnetic torque equation is:

$$T_e = 1.5 p_n \begin{bmatrix} \psi_\alpha & \psi_\beta \end{bmatrix} J^T \begin{bmatrix} i_\alpha & i_\beta \end{bmatrix}^T \tag{53}$$

The output y of the system can be measured, so the minimum-order state observer is designed to observe the extended flux linkage. The observer model is:

$$\dot{\hat{x}} = A\dot{x} + Bu + K[y - \hat{y}] \tag{54}$$

Where: K is the state observer feedback matrix. The state observer is constructed according to the state equation, and the state variable is selected as the extended flux linkage $\psi_{\alpha \beta 1}$.

$$\begin{cases} x = \psi_{\alpha \beta 1} \\ \dot{x} = D\psi_{\alpha \beta 1} \end{cases} \tag{55}$$

According to the above formula, the minimum-order state observer of the extended flux linkage is:

$$\begin{cases} \dot{\hat{x}} = D\hat{\psi}_{\alpha \beta 1} \\ \quad = \hat{y} + K(y - \hat{y}) \\ \quad = \omega_e J \hat{\psi}_{\alpha \beta 1} + K(u_{\alpha \beta} - R_s i_{\alpha \beta} - LDi_{\alpha \beta} - \omega J \hat{\psi}_{\alpha \beta 1}) \\ \hat{y} = \omega_e J \hat{x} = \omega_e J \hat{\psi}_{\alpha \beta 1} \end{cases} \tag{56}$$

The error equation for the state observer is:

$$
\begin{aligned}
D\widetilde{\psi}_{\alpha\beta1} &= (A - KC)(\hat{x} - x) \\
&= \omega(1 - K)J(\hat{\psi}_{\alpha\beta1} - \psi_{\alpha\beta1})
\end{aligned}
\tag{57}
$$

Where: $\widetilde{\psi}_{\alpha\beta1}$ is used to expand the observation error of the observation flux linkage.

It can be seen from the above formula that by performing pole placement on the feedback matrix K, the state observer based on the extended flux linkage can be converged, and the convergence speed is guaranteed to be within a reasonable range. The control block diagram of the extended flux observer is shown in Figure 4:
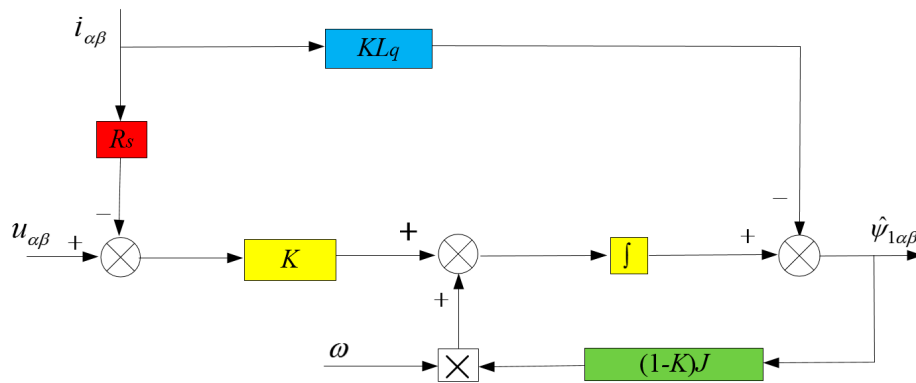
Figure 4. Extended flux observer.

The system structure block diagram as shown in Figure 5:
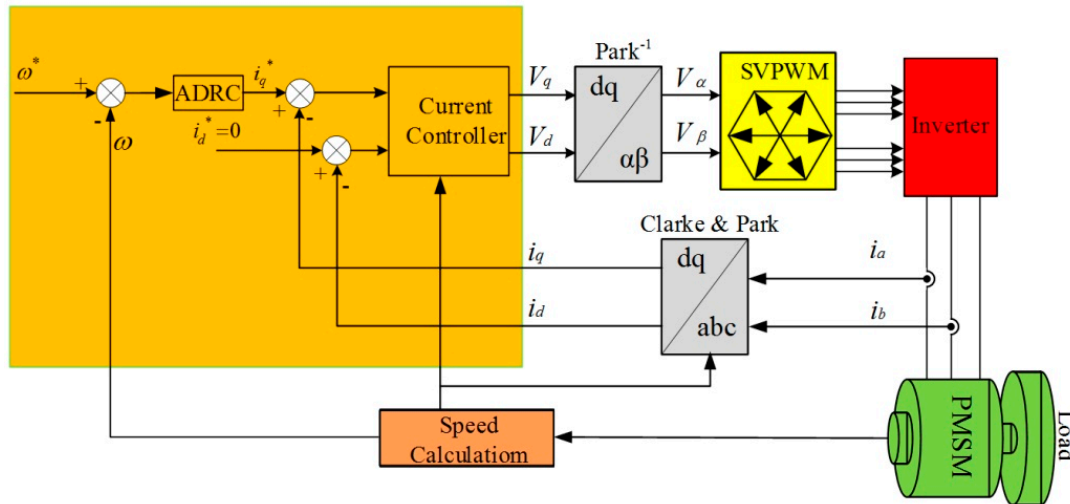
Figure 5. System block diagram.

5. System Simulation Experiment

During the simulation and testing of the system, the parameters of the PMSM are shown in Table 1, and the parameters of the controller are shown in Table 2.

Table 1. PMSM parameters.

Parameter	Value
Rated power/(kW)	1.28
Rated speed/(r/min)	2000
Rated torque/(N·m)	75
Polar logarithm	4
Moment of inertia/(kg·m^2)	1.469×10^{-3}
L_d, L_q/(H)	0.00334
Permanent magnet flux linkage/(Wb)	0.171

Table 2. Controller parameter.

Parameter	Value
r	2×10^6
ω_0	1400
β_1	2800
β_2	1.69×10^6
k	0.6
b	698.4
α_1	4720
α_2	1910

The simulation experiment is carried out under ideal conditions, it mainly includes speed loop and current loop.

Simulation of the speed loop:

(a) When the speed is $n = 1000$ r/min, the no-load starts and no disturbance is recorded during the entire process.

Figure 6 reveals that the speed waveform has obvious overshoot when using the PI controller. Additionally, oscillation is significant during the initial stage of the motor starting, and the transition time is long; meanwhile the ADRC controller has no overshoot, a short transition time, and quick response. In short, the motor starts smoothly.

(b) When the speed $n = 1000$ r/min, the no-load starts, and the torque rises to 2 N·m when $t = 30$ ms.

(c) When the speed $n = 1000$ r/min, the torque drop of the 2 N·m torque start at $t = 30$ms is equal to 0 N·m.
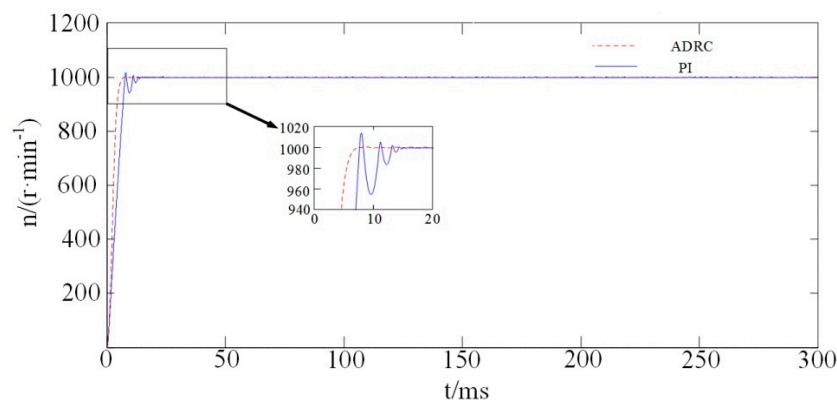
Figure 6. Response waveform at 1000 r/min.

The simulation of the anti-disturbance performance of the ADRC and PI controller are recorded in Figures 7 and 8. As shown, when the load is applied or reduced after the motor is running in a stable manner, the dynamic effect of the ADRC controller speed waveform is superior to that of the PI controller. The advantage is in the fact that the ADRC is shorter than the PI following the disturbance

to the steady state, meaning that the change in the rotational speed caused by the sudden alteration of the load is small, resulting in stronger anti-disturbance capabilities.
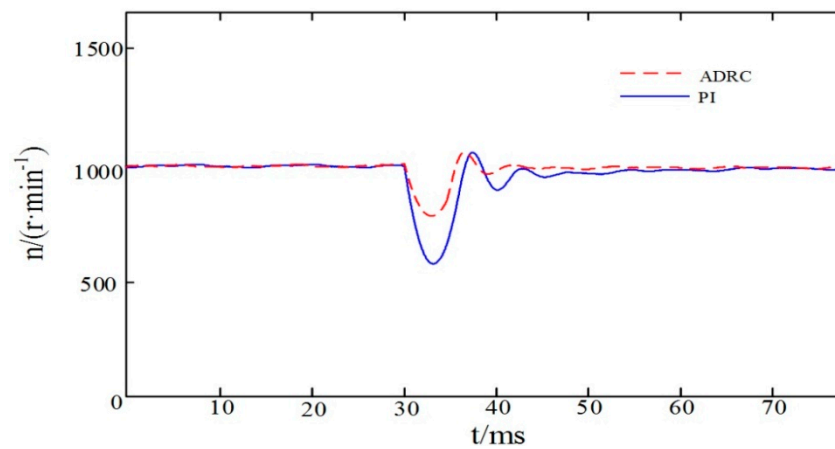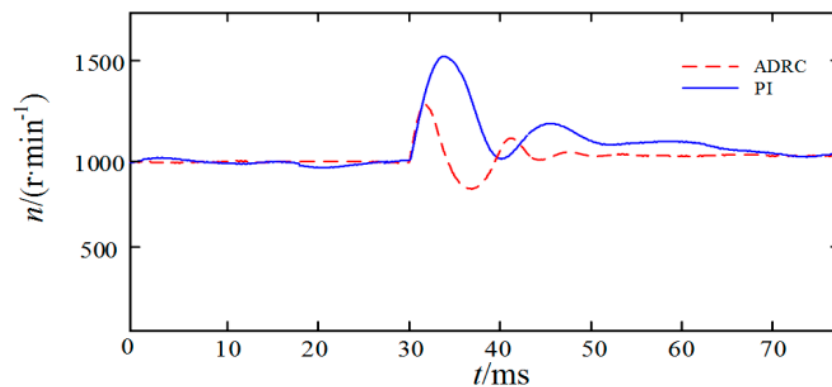

Figure 7. Response waveform.

Figure 8. Response waveform at t = 0.3 s torque decrease to 0 N·m.

(d) When the rotational speed n = 1000 r/min, the electromagnetic torque waveform is shown in Figure 9. It can be seen from the figure that its starting torque overshoot is smaller, and the transition is faster when the load is suddenly applied.

Current loop simulation:

Load simulation, at 1000 r/min, 2 N·m at 0.2 s, and 2 N·m at 0.4 s, the current loop q–axis current response waveform controlled by the current controller and the PI is shown in Figure 10. In the dynamic process of load disturbance, the current overshoot of the current controller is significantly smaller than that of the PI controller, and it can enter a stable operation state in a short time in the face of load changes.
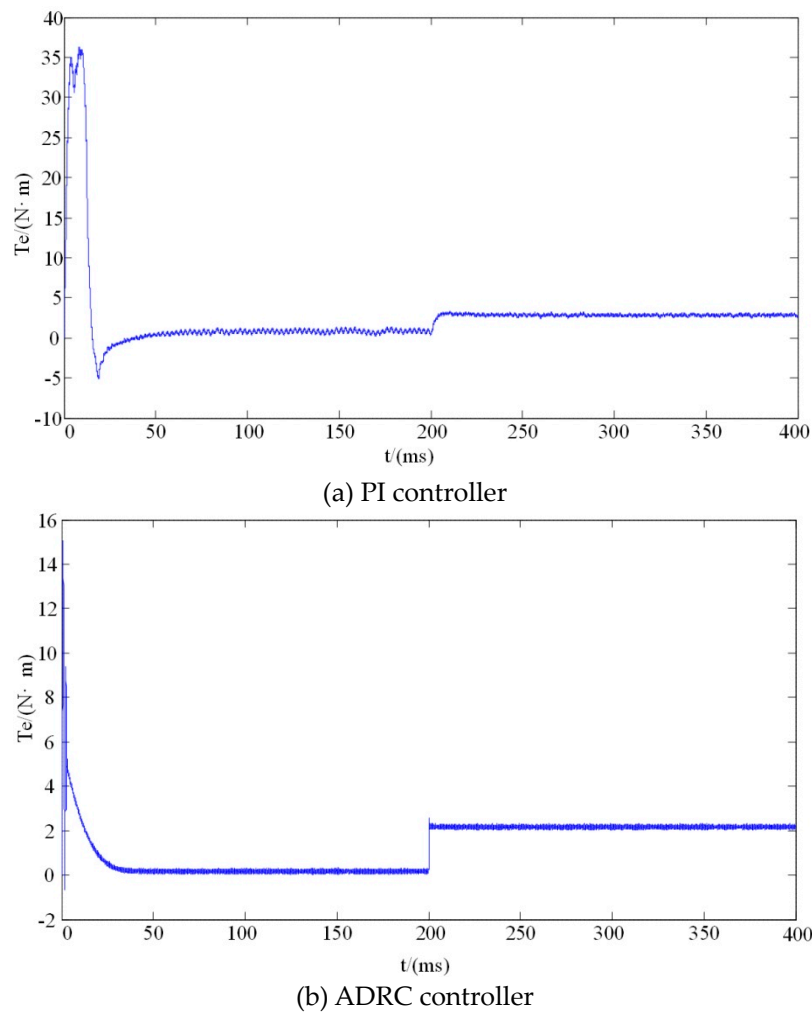
(a) PI controller

(b) ADRC controller

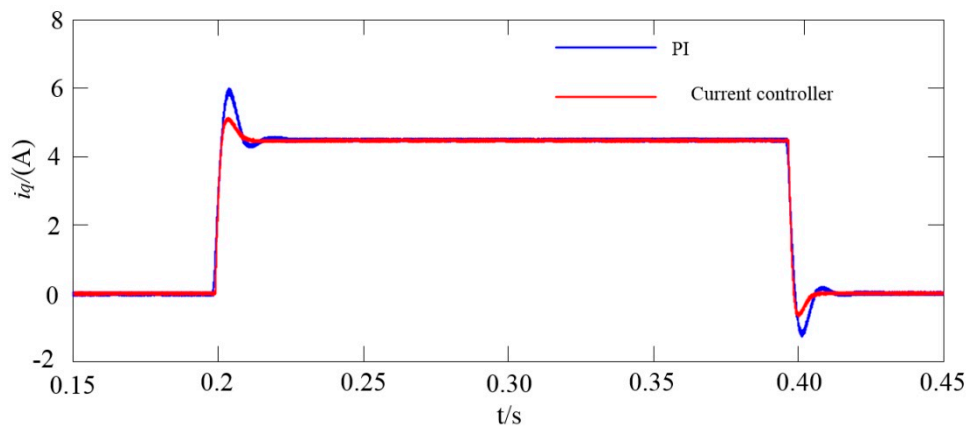**Figure 9.** The electromagnetic torque waveform.

Figure 10. The current response in the loading of the q–axis.

6. Experimental Verification

The system experiment platform is mainly composed of the PMSM motor, motor controller and host computer. The experimental platform can complete the collection of important information such as torque, rotation, voltage and current curve and power of the motor. The experimental platform of the motor drive control system is shown in Figure 11.
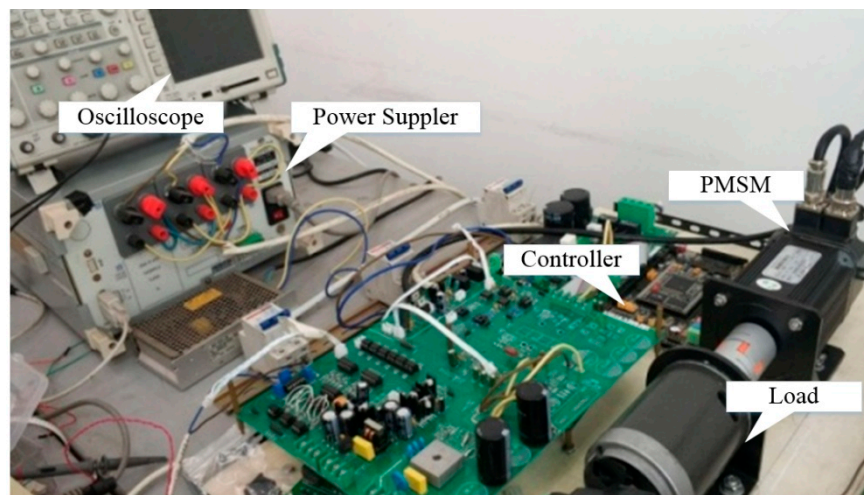
Figure 11. Test Platform.

In order to verify that the control system has no overshooting response, the motor is unloaded and started at 1000 r/min. The results are shown in Figure 12, which reveals that under the same conditions the ADRC control quickly reaches the desired speed without causing the system overshoot. The overshoot of the PI controller is more obvious, and it will stabilize in 300 ms.
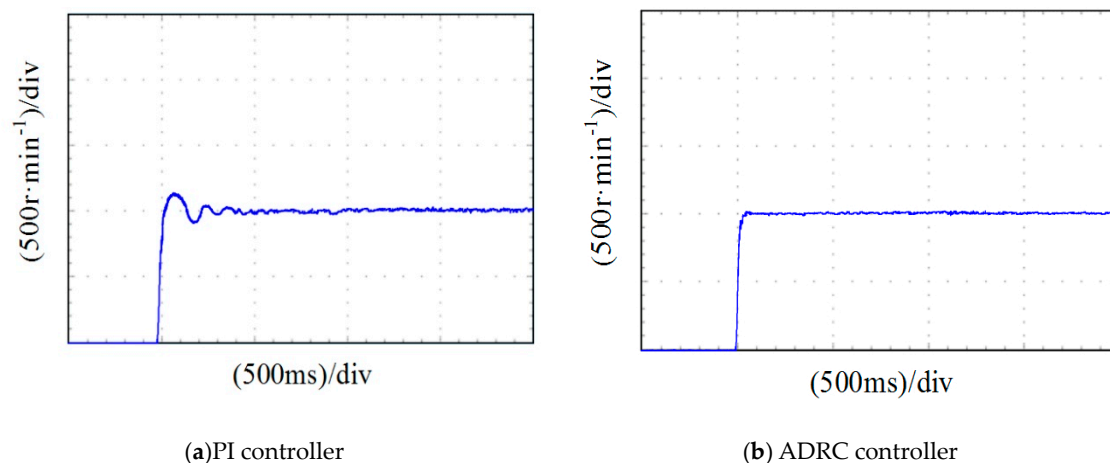

(**a**)PI controller

(**b**) ADRC controller

Figure 12. Speed waveform at 1000 r/min.

In order to verify the accuracy of our load changes, the initial load torque was zero, and became 2 N·m at 700 ms. Then uninstall to 0 N·m. The image of the PMSM speed is shown in Figures 13 and 14. Comparing the these figures, it can be observed that under the ADRC controller that the speed of the system recovered more quickly following a disturbance, and the speed suffered less of a drop-off. The PI controller takes about 600 ms to recover, and the ADRC can be recovered in less than 300 ms. The experimental results are basically consistent with the simulation results. The current response curves of the q–axis during loading and unloading are shown in Figures 15 and 16. The current overshoot of the q–axis is smaller and the recovery time is faster. When loading, the PI controller takes about 8 ms to stabilize, and the current controller only needs about 4 ms to stabilize. The peak voltage of the PI controller is 1.5 A larger than the current controller. The overall result is generally consistent with the simulation. Therefore, the ADRC has a more desirable control effect on the PMSM.
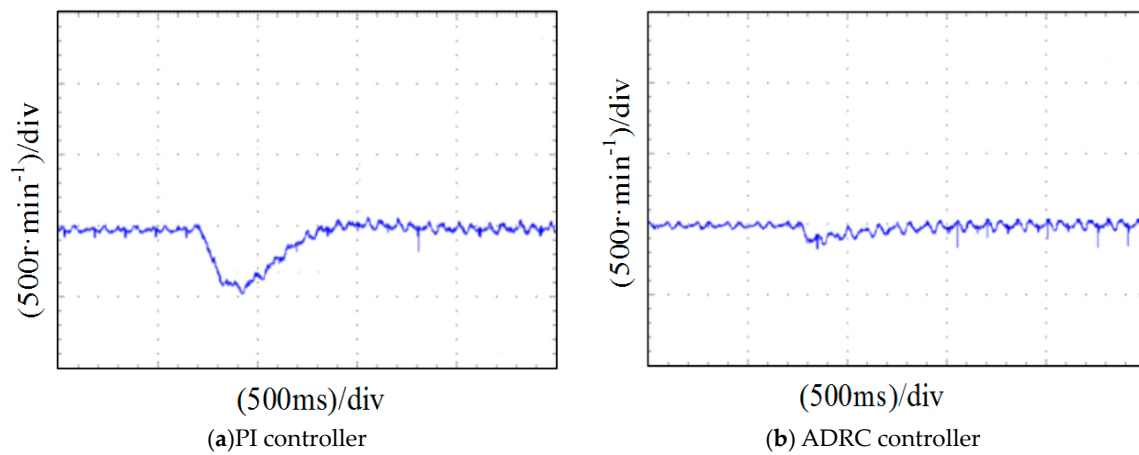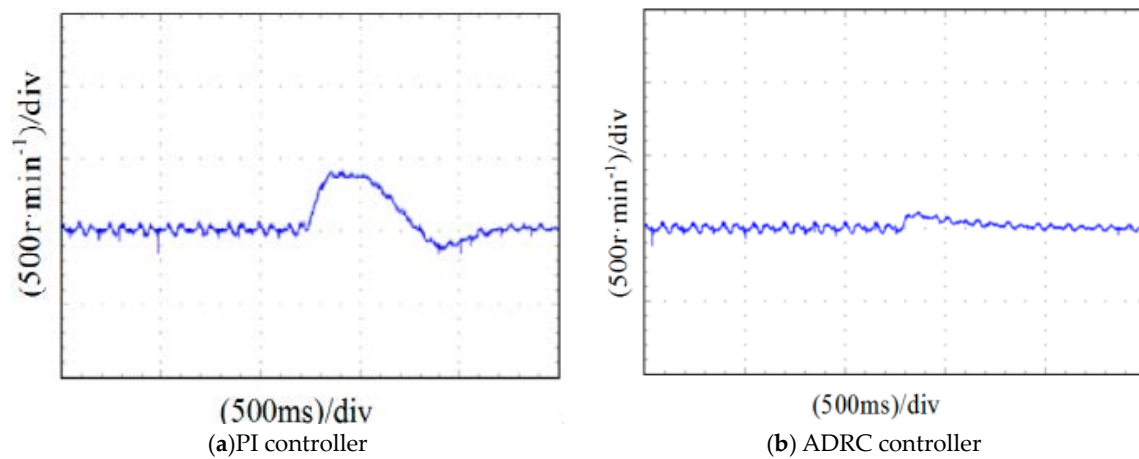
(**a**)PI controller   (**b**) ADRC controller

Figure 13. Response waveform.

(**a**)PI controller   (**b**) ADRC controller

Figure 14. Speed response curve when unloading.

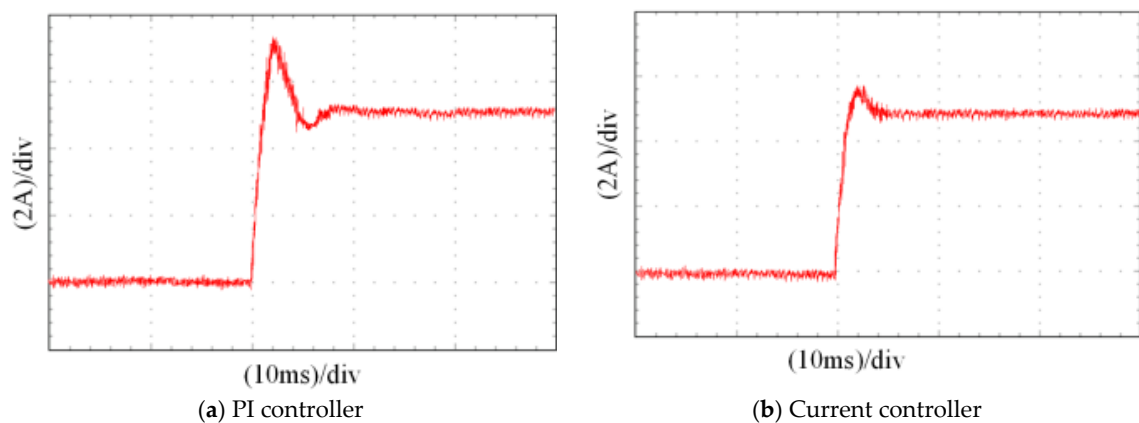(**a**) PI controller   (**b**) Current controller

Figure 15. The current response curve during loading of the q–axis.

The motor starting torque under the two control methods is shown in Figure 17. When the ADRC control strategy is used, the torque waveform is a triangular wave, which is different from the phenomenon that the PI controller is saturated. This is the result of the TD affecting the transition process.
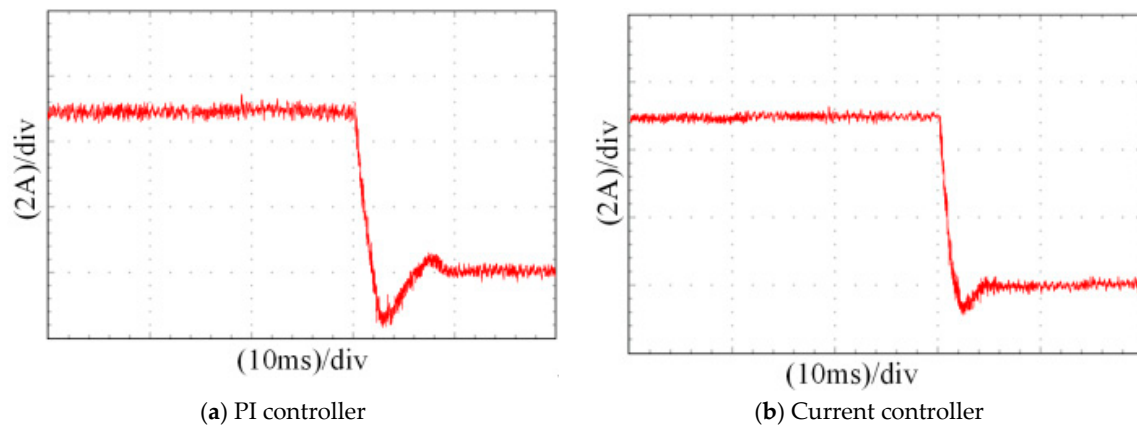
(**a**) PI controller　　　　　　　　　　　　　(**b**) Current controller

Figure 16. The current response curve during unloading of the q–axis.

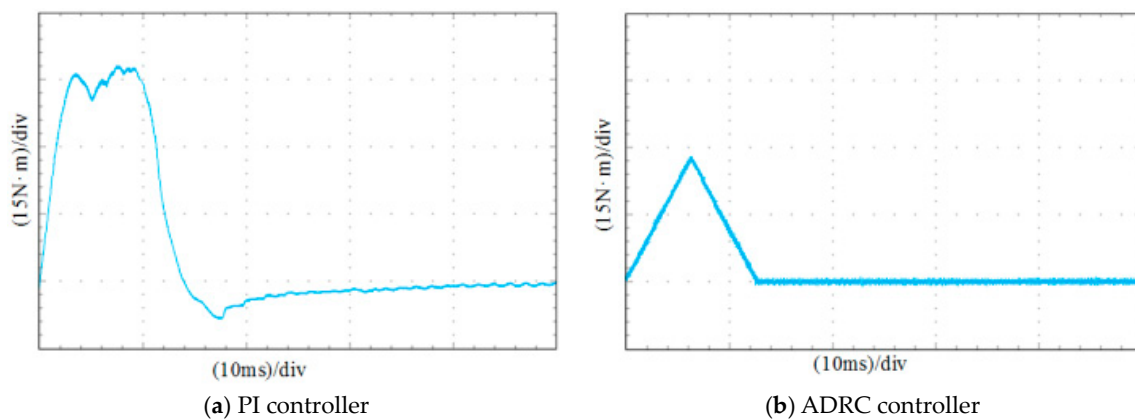(**a**) PI controller　　　　　　　　　　　　　(**b**) ADRC controller

Figure 17. Starting torque waveform.

7. Conclusions

This paper proposes an active disturbances rejection control technology as the PMSM speed loop controller. It does not fully depend on the controlled object model. The variation of moment of inertia, stator resistance and other unknown disturbances are measured and compensated for by the ADRC speed loop, making the system strong against system parameter changes and external disturbances.

In order to achieve decoupling the complex coupling term of the PMSM, the feedback linearization algorithm is used to optimize the controller, and the decoupling control of the system is realized. The simulation and experimental research on the control system show that the control strategy has strong robustness, and the dynamic tracking performance is stable and accurate.

Author Contributions: K.Z. and M.A. conceived and designed the experiments; Y.S. performed the experiments; X.W. analyzed the data; R.L. wrote the paper.

Conflicts of Interest: The authors declare no conflict of interest.

References

1.　Liu, J.; Li, H.; Deng, Y. Torque Ripple Minimization of PMSM Based on Robust ILC Via Adaptive Sliding Mode Control. *IEEE Trans. Power Electron.* **2018**, *33*, 3655–3671. [CrossRef]

2.　Liu, Y.; Cheng, S.; Ning, B.; Li, Y. Robust model predictive control with simplified repetitive control for electrical machine drives. *IEEE Trans. Power Electron.* **2019**, *34*, 4524–4535. [CrossRef]

3. Yu, J.; Chen, B.; Yu, H.; Lin, C.; Ji, Z.; Cheng, X. Position tracking control for chaotic permanent magnet synchronous motors via indirect adaptive neural approximation. *Neurocomputing* **2015**, *156*, 245–251. [CrossRef]

4. Wang, T.; Huang, J.; Ye, M.; Chen, J.; Kong, W.; Kang, M.; Yu, M. An EMF Observer for PMSM Sensorless Drives Adaptive to Stator Resistance and Rotor Flux-linkage. *IEEE J. Emerg. Sel. Top. Power Electron.* **2019**, *7*, 1899–1913. [CrossRef]

5. Lin, F.J.; Sun, I.F.; Yang, K.J.; Chang, J.K. Recurrent Fuzzy Neural Cerebellar Model Articulation Network Fault-Tolerant Control of Six-Phase Permanent Magnet Synchronous Motor Position Servo Drive. *IEEE Trans. Fuzzy Syst.* **2016**, *24*, 153–167. [CrossRef]

6. Kouro, S.; Cortes, P.; Vargas, R.; Ammann, U.; Rodriguez, J. Model Predictive Control—A Simple and Powerful Method to Control Power Converters. *IEEE Trans. Ind. Electron.* **2009**, *56*, 1826–1838. [CrossRef]

7. Chai, S.; Wang, L.; Rogers, E. A Cascade MPC Control Structure for a PMSM with Speed Ripple Minimization. *IEEE Trans. Ind. Electron.* **2013**, *60*, 2978–2987. [CrossRef]

8. Bolognani, S.; Bolognani, S.; Peretti, L.; Zigliotto, M. Design and Implementation of Model Predictive Control for Electrical Motor Drives. *IEEE Trans. Ind. Electron.* **2009**, *56*, 1925–1936. [CrossRef]

9. Wang, C.; Yang, M.; Zheng, W.; Long, J.; Xu, D. Vibration Suppression with Shaft Torque Limitation Using Explicit MPC-PI Switching Control in Elastic Drive Systems. *IEEE Trans. Ind. Electron.* **2015**, *62*, 6855–6867. [CrossRef]

10. Su, D.; Zhang, C.; Dong, Y. An Improved Continuous-Time Model Predictive Control of Permanent Magnetic Synchronous Motors for a Wide-Speed Range. *Energies* **2017**, *10*, 2051. [CrossRef]

11. Mohseni, M.; Islam, S.M.; Masoum, M.A.S. Impacts of symmetrical and asymmetrical voltage sags ondfig-based wind turbines considering phase-angle jump, voltage recovery, and sag parameters. *IEEE Trans. Power Electron.* **2011**, *26*, 1587–1598. [CrossRef]

12. Xiao, S.; Yang, G.; Zhou, H.; Geng, H. An lvrt control strategy based on flux linkage tracking for dfig-basedwecs. *IEEE Trans. Ind. Electron.* **2013**, *60*, 2820–2832. [CrossRef]

13. Shen, Y.; Cui, M.; Wang, Q.; Shen, F.; Zhang, B.; Liang, L. Comprehensive reactive power support of dfig adapted to different depth of voltage sags. *Energies* **2017**, *10*, 808. [CrossRef]

14. Jalilian, A.; Naderi, S.B.; Negnevitsky, M.; Hagh, M.T.; Muttaqi, K.M. Controllable dc-link fault current limiter augmentation with dc chopper to improve fault ride-through of dfig. *IET Renew. Power Gener.* **2017**, *11*, 313–324. [CrossRef]

15. Liu, Z.F.; Zhang, W.H.; Zhao, C.H.; Yuan, J.H. The economics of wind power in china and policy implications. *Energies* **2015**, *8*, 1529–1546. [CrossRef]

16. Yang, C.; Yang, X.; Tong, C. An ADRC based Control Strategy for FRT Improvement of Wind PowerGeneration with Doubly Fed Induction Generator. *Proc. CSEE* **2018**, *38*, 2487–2495.

17. Chakib, R.; Cherkaoui, M.; Essadki, A. Stator flux control by active disturbance rejection control for dfig wind turbine during voltage dip. *Int. J. Circuits Syst. Signal Process. (USA)* **2015**, *9*, 281–288.

18. Li, D.; Liu, L.; Jin, Q.; Hirasawa, K. Maximum sensitivity based fractional IMC-PID controller design for non-integer order system with time delay. *J. Process Control* **2015**, *31*, 17–29. [CrossRef]

19. Xue, W.; Huang, Y. Performance analysis of active disturbance rejection tracking control for a class of uncertain LTI systems. *ISA Trans.* **2015**, *58*, 133–154. [CrossRef]

20. Tohidi, A.; Hajieghrary, H.; Hsieh, M.A. Adaptive disturbance rejection control scheme for dfig-based wind turbine: Theory and experiments. *IEEE Trans. Ind. Appl.* **2016**, *52*, 2006–2015. [CrossRef]

21. Han, J. *The Technique for Estimating and Compensating the Uncertainties: Active Disturbance Rejection ControlTechnique*; National Defense Industry Press: Beijing, China, 2008.

22. Herbst, G. Practical active disturbance rejection control: Bumpless transfer, rate limitation, and incremental algorithm. *IEEE Trans. Ind. Electron.* **2016**, *63*, 1754–1762. [CrossRef]

23. Song, Z.; Mei, X.; Jiang, G. Inertia identification based on model reference adaptive system with variable gain for AC servo systems. In Proceedings of the ICMA 2017 IEEE International Conference on Mechatronics and Automation, Takamatsu, Japan, 6–9 August 2017; pp. 188–192.

24. Liu, Z.; Yang, M.; Xu, D. A novel algorithm for on-line inertia identification via adaptive recursive least squares. In Proceedings of the IECON 2017—43rd Annual Conference of the IEEE Industrial Electronics Society, Beijing, China, 29 October–1 November 2017; pp. 2973–2978.

25. Niu, L.; Xu, D.; Yang, M.; Gui, X.; Liu, Z. On-line Inertia Identification Algorithm for PI Parameters Optimization in Speed Loop. *IEEE Trans. Power Electron.* **2015**, *30*, 849–859. [CrossRef]

26. Lyu, M.; Wu, G.; Luo, D.; Rong, F.; Huang, S. Robust Nonlinear Predictive Current Control Techniques for PMSM. *Energies* **2019**, *12*, 443. [CrossRef]

27. Lesprier, J.; Roos, C.; Biannic, J.; Morari, M. Improved μ upper bound computation using the μ -sensitivities. *IFAC-PapersOnLine* **2015**, *48*, 215–220. [CrossRef]